Applied Physics A (2020) 126:756
https://doi.org/10.1007/s00339-020-03933-4

Applied Physics A
Materials Science & Processing

Elastomeric polydimethylsiloxane polymer on conductive interdigitated electrode for analyzing skin hydration dynamics

Santheraleka Ramanathan[1] · M. Jusoh[2] · T. Sabapathy[2] · M. N. Yasin[2,3] · Subash C. B. Gopinath[1,4] · H. ARahim[2] · M. N. Osman[2] · Y. Abdul Wahab[5]

Received: 8 June 2020 / Accepted: 20 August 2020 / Published online: 31 August 2020

Abstract
With an approach towards generating a wearable skin hydration detecting system, simple, cheap, and flexible skin hydration sensing strategy was demonstrated here using an interdigitated electrode (IDE) coated with polydimethylsiloxane (PDMS) matrix. Aluminium IDE with a 400 µm gap and 250 µm electrode sizes were fabricated using a photolithography method. Morphological characterizations were performed using a high power microscope, 3D-profilometer, and scanning electron microscope. The dimensions of electrodes and gaps measured through electron microscopic analysis affirmed the exactness of IDE and the fabrication process. After coated with PDMS polymer, the IDE/PDMS surface was examined under a high power microscope and 3D-profilometer. The optical characterization revealed the polymer was coated on IDE through the color-shade changes and smooth surface observed under an optical microscope and the respective 3D-visualization. IDE/PDMS was also analyzed by an atomic force microscope, revealing the smoothness of the IDE surface. Electrical characterizations were performed using different pH and urea solutions and the sweat to investigate the influence of real-time and artificial sweat on IDE/PDMS. As the device showed appropriate results with real-time sweat and no effect with artificial interferences, it is highly encouraged and recommended for detecting skin hydration and the related illnesses with the point-of-care concept.

Keywords Skin sensor · Optical characterization · Skin hydration · Sweat

1 Introduction

The skin has the capability of changing its structure and returning to the normal, can be an indication of lacking hydration or liquid pick-up. It is a consequential condition especially with kids and older people [1, 2]. The common sicknesses like cardiovascular disease, diabetes, and malignant growth can be related to different skin hydration levels [3]. Thus, effortless and efficient detection strategies for skin hydration are important. Sweat is an efficient electrolytic solution excreted from the human body that can be used to measure skin hydration at the instant time [4, 5]. The sweat excreted due to the physical properties of skin such as capacitance, conductance, impedance, the reflectance of optical or electromagnetic radiation and thermal conductivity, justifies the correct results on the water level in the human body [6]. The non-invasive clinical sampling of human sweat is highly recommended for the detection strategy of skin hydration as it detects the real-time skin hydration without any invasive injections [7].

Although body hydration is classified as a significant parameter for measuring physiology, it is still difficult to evaluate correctly. Initially, body dehydration is determined qualitatively through the appearances of a person, such as dried lips and sunken eyes [8]. Later on, the dehydration level is determined quantitatively by measuring the

✉ M. Jusoh
muzammil@unimap.edu.my

1 Institute of Nano Electronic Engineering, Universiti Malaysia Perlis, 01000 Kangar, Perlis, Malaysia

2 Advanced Communication Engineering (ACE) Centre of Excellence, School of Computer and Communication Engineering, Universiti Malaysia Perlis, Campus Pauh Putra, 02600 Arau, Perlis, Malaysia

3 School of Microelectronic Engineering, Universiti Malaysia Perlis, Campus Pauh Putra, 02600 Arau, Perlis, Malaysia

4 School of Bioprocess Engineering, Universiti Malaysia Perlis, 02600 Arau, Perlis, Malaysia

5 Nanotechnology and Catalysis Research Centre, Deputy Vice Chancellor (Research and Innovation) Office, University of Malaya, Kuala Lumpur, Malaysia

physical properties of skin such as impedance, capacitance, and skin radiation. However, those quantitative techniques need high-cost equipment and well-trained expertise to handle [9]. Hydration sensors that are mechanically compatible and can form a comforting contact with the skin are the major technological advances to replace the costly and bulky instruments and attain low-cost, long-term hydration surveillance [10, 11]. Conventional sweat assessment methodologies include collection using skin-taped gauze pads, then chemical compositional determination with benchtop instruments are performed accordingly [12]. While useful in clinical contexts and laboratory, these approaches unable to give real-time information, and their precision has been restricted by sample contamination, loss, and degradation during multi-stage collection, storage, transportation, and evaluation procedures [13]. Alternate approaches are electrochemical potentiometric and amperometric methods to use hydration sensors for a real-time skin assessment.

The present research proposes the leverage to competence in biosensing, formation of realistic tissue phantoms, and displaying and signal handling, and accessing a wearable point-of-care (POC) device for tracking the hydration/dehydration levels of the skin. Varieties of proposed noninvasive optical wearable innovations could be utilized to give the extra knowledge into patient wellbeing and empower the early intercession when required. Due to the enhanced interest in sweat clinical use, multiple approaches with sweat samplings have been recorded and analyzed. Towards that, the present research reports the simple, cheap, and flexible skin hydration sensing system using an interdigitated electrode (IDE) coated with polydimethylsiloxane (PDMS) matrix. The PDMS matrix is used in detecting skin hydration as it maintains a good chemical resistance, thermal stability, and mechanical flexibility contact on the skin [14, 15]. The research also ensures that the IDE-based hydration sensor is able to detect sweat without external influences. Figure 1 demonstrates the overall concept of PDMS-based IDE in detecting skin hydration/dehydration through the non-invasive sensors.

2 Materials and methods

2.1 Materials

Silicon wafer for IDE fabrication was procured from Mallinckrodt Baker, Inc (USA). Futurrex, Inc (USA) was reached to purchase resist developer, RD6 and positive photoresist and PR+ solutions. Aluminium coil and aluminium etch solution for deposition and etching, respectively were purchased from Sigma Aldrich (USA), together with other analytical solutions used in the research. PDMS polymer

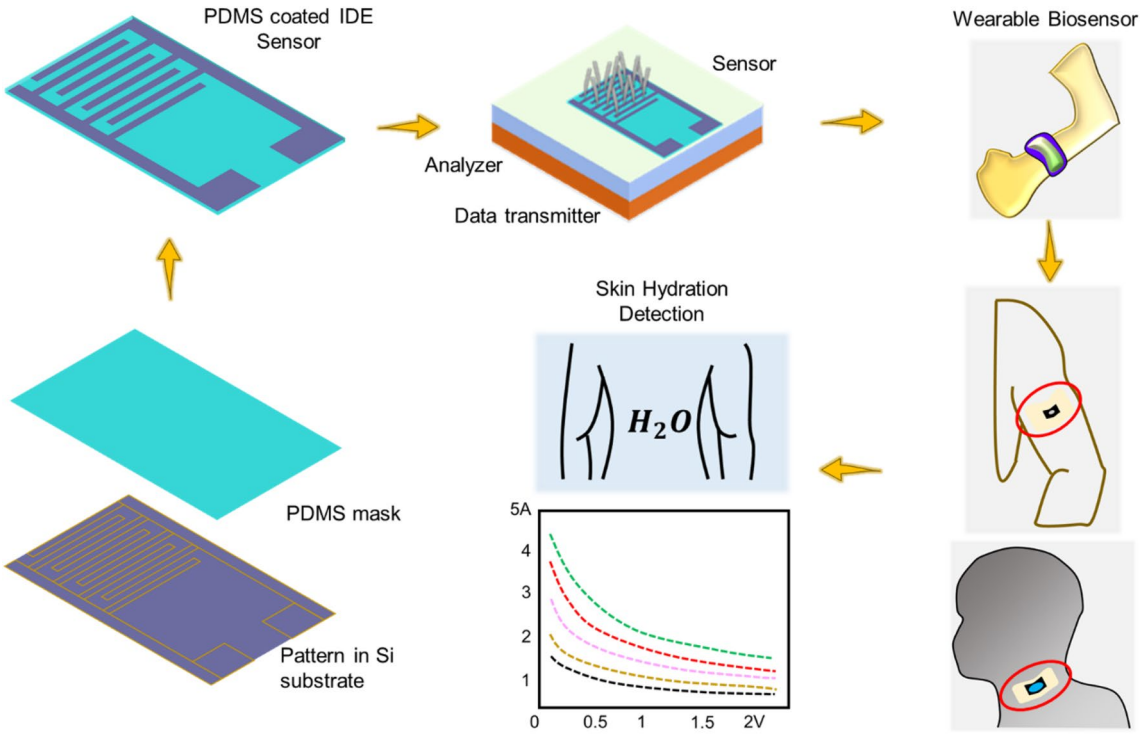

Fig. 1 Schematic illustration represents the development of PDMS coated IDE in detecting skin hydration with the approach of generating a wearable sensor

with its curing agent was also procured from Sigma Aldrich (USA).

2.2 Fabrication of IDE/PDMS with conductive aluminium electrodes

Pattern of device design was designed using AutoCAD and transferred onto a chrome mask. Silicon substrate (wafer) was oxidized under the wet thermal oxidation at 500 °C using chemical vapor deposition (CVD) to create 300 Å oxide layer. Aluminium (Al) metal was deposited on the oxidized wafer using physical vapor deposition (PVD). The aluminium deposited wafer was used for the photolithography process to fabricate IDE. Positive photoresist (PR) was coated on the Al layer using the spin coating method and soft-baked at 90 °C for 2 min. IDE mask was aligned with a substrate surface and allowed under UV-light exposure for 10 s to transfer the IDE pattern on the photoresist layer. Then, RD developer was used to removing the existed positive photoresist on the UV unexposed area. The developed electrode pattern was examined under a high power microscope (HPM) to ensure the accurate pattern development. Then, hard-bake was done for 1 min at 110 °C to evacuate the undesirable dampness and improve the adhesion power between the Al and SiO_2 layers. Then unexposed Al layer was evacuated by drenching in Al etchant for 1 min [16–18]. Finally, sample was cleaned using acetone and distilled water to remove the photoresist. The fabricated IDE was analyzed under HPM, 3D-profilometer, and scanning electron microscope (SEM) to verify the accuracy of device fabrication. To coat PDMS on IDE, PDMS polymer was prepared by mixing PDMS prepolymer with curing agent at 10:1 weight ratio. The mixture was mixed well continuously for 15 min. Fabricated IDE was placed on the spin coater and the well-mixed PDMS was poured on the IDE as it covers the entire surface. A uniform layer of PDMS was coated on the IDE surface by spin coating at 3000 rpm for 50 s. The PDMS coated IDE was baked at 70 °C for 4 h. Figure 2 shows a schematic illustration of fabricating IDE using the photolithography technique and the final structure of the fabricated device. IDE with 400 µm Al electrode and separated by 250 µm gap is firm and rigid. The silicon substrate acts as the base element of IDE ensures the final device is stern and firm. The final structure of the device and its cross-sectional view is shown in Fig. 2. The PDMS was coated as it occupies the entire top surface of the IDE. In a probe station, the electrode probes were placed precisely on the two electrode pads of IDE and the current–voltage characterization is performed. The sensing was performed without removing the PDMS layer once coated. The IDE/PDMS layer was analyzed by 3D-profilometer, HPM and atomic force microscope (AFM, NanoScope, Ica, Veeco, USA) to examine the surface characterization.

2.3 Surface morphological analysis

Fabricated aluminium IDE was observed through optical microscopes. A high power microscope was utilized to examine the surface of IDE electrodes and gaps. The uniformity of surface thickness was analyzed with a 3D-profilometer (WT-250 Series, Hawk 3D Nano-Profiler, Korea) reveling the 3D-vision of IDE. The morphology of IDE was further examined under the scanning electron microscope (SEM, JEM-2100F, JEOL, Japan). The dimensions of IDE electrodes and gaps were measured using the SEM measuring tool, which justified the precision of IDE. Once IDE coated with PDMS polymer, the IDE/PDMS was observed under HPM and 3D-profilometer indicating polymer layer on IDE with variation in surface thickness and smoothness.

2.4 IDE/PDMS electrical characterization

Fabricated IDE/PDMS device was analyzed to determine the reproducibility and its influence with artificial skin excretes. The electrical signal generated by the device at the variant sampling solvent was monitored by Picoammeter. The voltage was set from 0 to 2 V and both positive and negative terminal probes were kept in contact with the electrode pad of IDE/PDMS. To test the reproducibility, the device was tested with pH 4, pH 5, and pH 6 since the pH of human sweat is ranging from pH 5 to pH 6. Then, the device was further analyzed with urea, where its concentration ranges at 10 mM, 20 mM, 30 mM, and 40 mM. Since the concentration of urea in human sweat is ~ 22 mM, urea with the above concentrations were prepared and tested on IDE/PDMS. The influence of human sweat on IDE/PDMS was examined. A 10 µL of human sweat was added on the IDE/PDMS sensing surface and the electric signal generated by Picoammeter was recorded. The results were compared to investigate the variation between artificial and natural human sweats.

3 Results and discussion

The research encloses the fabrication of the IDE device using the photolithography technique and the accuracy was verified with electron and optical characterization. Moreover, to empower the device for detecting skin hydration, PDMS polymer layer was coated on the sensing surface. The IDE/PDMS was characterized by optical and electrical characterizations.

3.1 Characterization of interdigitated electrode (IDE)

3.1.1 High power microscope (HPM)

The IDE design was modelled as shown in Fig. 3, as it is suitable for the detection of skin hydration/dehydration

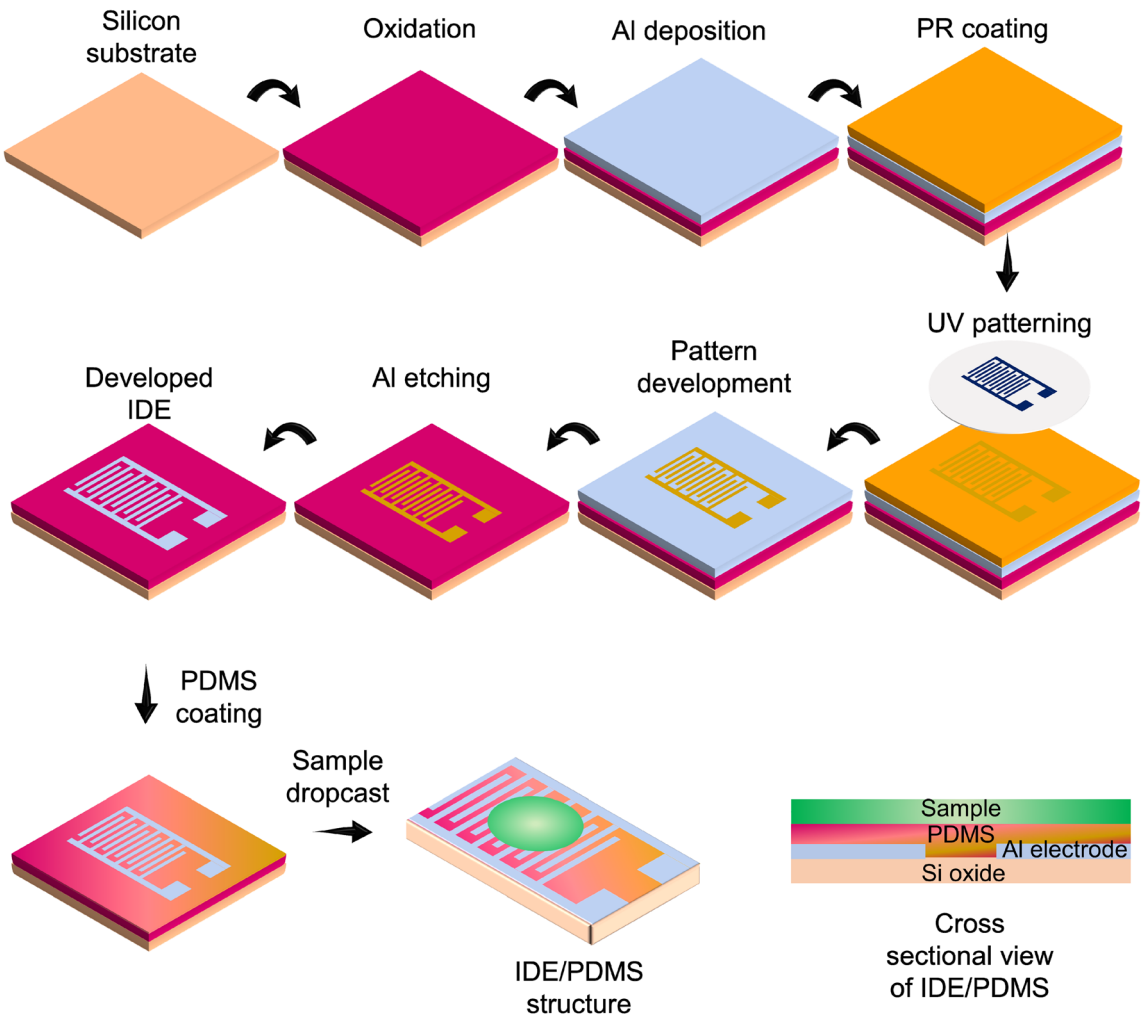

Fig. 2 Schematic illustration of fabricating IDE and development of IDE/PDMS. The figure illustrates the final structure and cross-sectional view of IDE/PDMS for detecting skin hydration levels

based on the water content. The device content with 20 aluminium electrodes is known as fingers and the remaining area known as the gap, where the SiO_2 layer was exposed. The fabricated IDE was observed under HPM to justify the measurements and connections of electrodes and gaps for the current flow through the device. Figure 3a and b show the electrodes and the junction of the device, respectively through the blue film of HPM. The image observed under the microscope affirms the precision in the device fabrication, as there were no misconnections between the electrodes. Figure 3c and d indicate the image of the device captured under dark films, where the dimension of electrodes and gap were measured.

3.1.2 Scanning electron microscope (SEM)

The fabricated IDE was observed under SEM to further affirm its dimension. Figure 3e and f show the image of IDE captured under SEM and the dimensions of electrodes and gap were measured using the microscope-measuring tool. At 500 µm scale, the image of IDE was clearly observed. The dimensions of the device measured under SEM were in good agreement with the designed IDE dimension, which implies the flawlessness with fabrication. The variation in the dimension measured was ~ 10 µm.

3.1.3 3D-profilometer

Optical imaging of IDE under 3D profilometer demonstrates the smoothness and height of the device. Figure 4a–c show the optical images of aluminium gaps, electrode and junction of IDE, respectively demonstrates the smoothness of the sensing surface. Figure 4d–i represent the 3D images of IDE at variant angles. The differences in the color of images appeared to indicate the thickness of the device. The uniform orange and blue color imply, electrodes and gaps

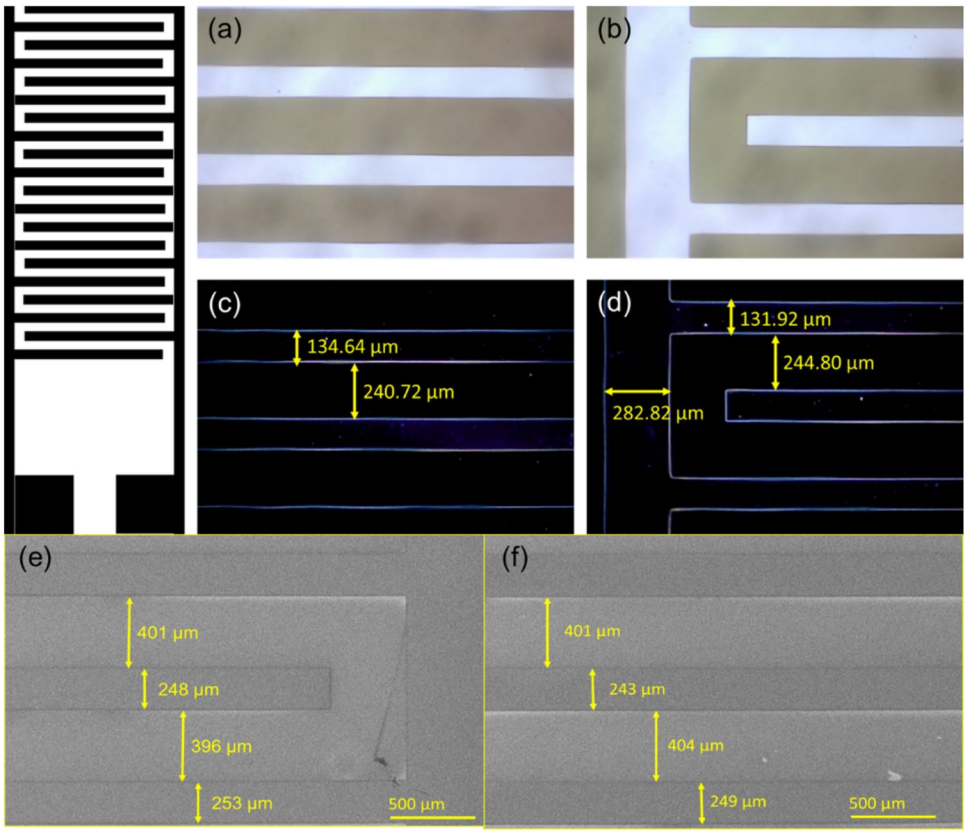

Fig. 3 Characterization of aluminium IDE. Design of IDE developed is shown. HPM images of **a** electrode fingers and **b** electrode junction. Optical images **c** and **d** represent the electrode finger and junction, respectively under the dark film of HPM characterization with electrode measurements. SEM analysis of fabricated IDE is shown in **e** and **f** with measurements of dimension indicating the exactness of IDE as well as fabrication technique

respectively affirm its uniform thickness of IDE. Based on the Hawk 3D surface analysis, the maximum height of Al electrode is ~ 4 µm. Moreover, the clean surface implies the presence of very least impurities on the IDE surface [19].

3.2 Characterization of IDE/PDMS

3.2.1 High power microscope (HPM)

PDMS coated IDE was examined under HPM. Figure 5a–c shows the optical image of IDE/PDMS is revealing the appearance of a polymer layer on top of the device. The viscous PDMS layer on IDE was observed as the electrode and gap appear as white and purple color compared to the clear grey aluminium electrode and blue gap (Fig. 3a and b).

3.2.2 3D-Profilometer

Figure 5d-f represents the optical images of IDE after being coated with PDMS. The sensing surface of IDE/PDMS was observed to be smooth, due to the elastic and flexible properties of PDMS polymer. The 3D vision of IDE/PDMS indicated from Fig. 5g–l convey the smooth and PDMS layer with uniform thickness, there is no obvious color variation between both electrode and gaps of IDE/PDMS. Based on 3D-profiler, the maximum height of PDMS coated IDE is 40 µm from its substrate level. By evaluating the maximum height difference of IDE and IDE/PDMS, the height of the elastomer layer is determined as ~ 10 µm. The height difference indicates the variation of surface roughness, indirectly resembling the variation in thickness between each surfaces [20]. The maximum thickness of IDE/PDMS is 40 µm and the Al electrode pattern is embedded under the elastomer layer. However, the light beam splitted on the device surface visualize the sample as a whole since PDMS layer is transparent. As illustrated in the cross-sectional view of IDE/PDMS in Fig. 2, PDMS layer covers the entire IDE [18, 21].

3.2.3 Atomic force microscope (AFM)

The gap between aluminium electrode before and after PDMS coating was examined under AFM to study its surface roughness. Figure 6a shows the top view of IDE gap revealing the presence of sharp particles, which are probably the impurities observed on the silicon oxide layer. Since the surface could be easily oxidized, the possibility for the oxide layer to be contaminated with metals and dirt is high and it is notable through the bright spots in Fig. 6a. The 3D view of the gap shown in Fig. 6b indicates the sharp ends of impurities present on the oxide layer of IDE. Surface analysis under AFM was emphasized that the maximum height of particles was spotted with 80 µm. After coated with PDMS,

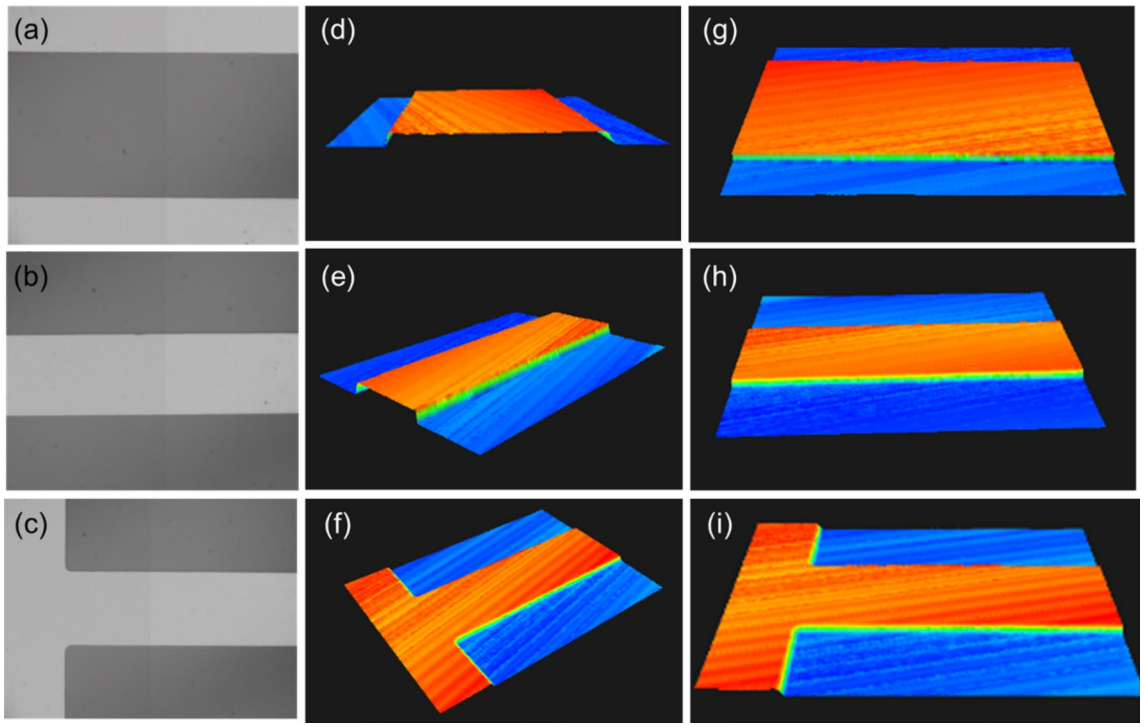

Fig. 4 Analysis of IDE under 3D profilometer. Optical images **a**, **b** and **c** represent the gap, electrode and junction of IDE, respectively. **d**–**i** Depicts the 3D view of IDE at various angles. The similarity in color of IDE surface is shown in 3D image illustrates the least variance in the thickness of aluminium electrode and the gaps

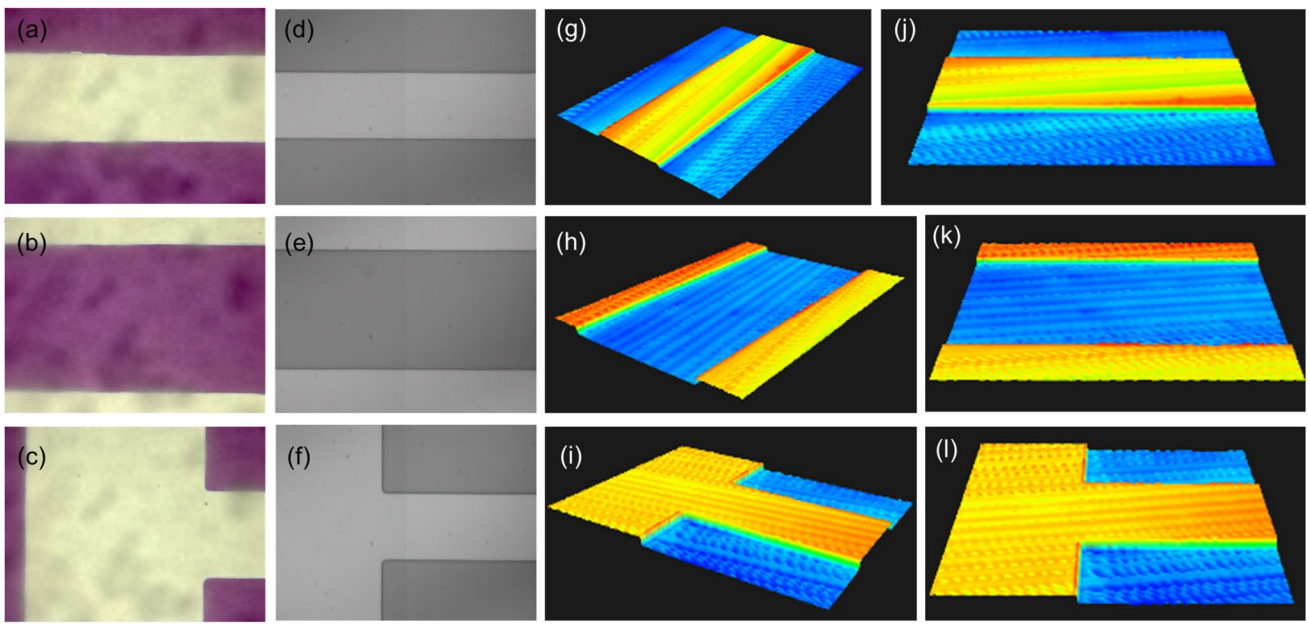

Fig. 5 Characterization of IDE/PDMS device. Images **a**, **b** and **c** show the PDMS coated IDE under HPM analysis. The polymer layer coated is affirmed through the color variation and the observed clumps of polymer particles on the IDE/PDMS surface. Optical images of IDE/PDMS under 3D profilometer are shown in **d**, **e**, and **f**, whereas images **g**–**i** reveal its 3D view. The images are arranged as the first, second and third rows represent electrode, the gap between electrode and electrode junction, respectively under HPM and 3D profilometer analyses

the images captured under AFM indicated a uniform smooth layer with no appealing particles observed (Fig. 6c). It is further justified with a 3D view of IDE/PDMS in Fig. 6d, resembling a smooth and uniform polymer layer. The smooth surface reveals the flexible PDMS elastomer which enables electrical sensing of biomolecules in a closed environment for detecting skin hydration.

3.3 Reproducibility of IDE/PDMS

PDMS based sensing platforms are well-established for their high piezoresistance sensitivity and flexibility, however, the sensing mechanism is yet to be explained [22]. The liquid polymer transforms into solid cross-linked elastomer upon baking. The PDMS elastomer acts as a substrate which creates an enclosed channel for sensing mechanisms to take place. Nanoscale electrodes may able to conduct the high electric field, however, it is poor in flexibility. To overcome such a challenge, flexible PDMS layer is coated on the sensing surface, which enables gas exchange or small molecules through invisible valves between two different media. This facilitates the study of cell locomotion, cell patterning, and indirectly improves the biocompatibility, and enables the electrical sensing of biomolecules in a confined space [23, 24]. Besides, the stretching of the elastomer in the presence of biomolecules or the sensing response with PDMS can be measured as piezoresistance. The piezoresistance of polymers specifies the stretching behavior with the change of electrical conductivity. Such analysis is often performed to validate the strength of elastomers in the sensing mechanism [25]. Although the sensing mechanism of PDMS is yet to be understood, the presence of PDMS elastomer enhances

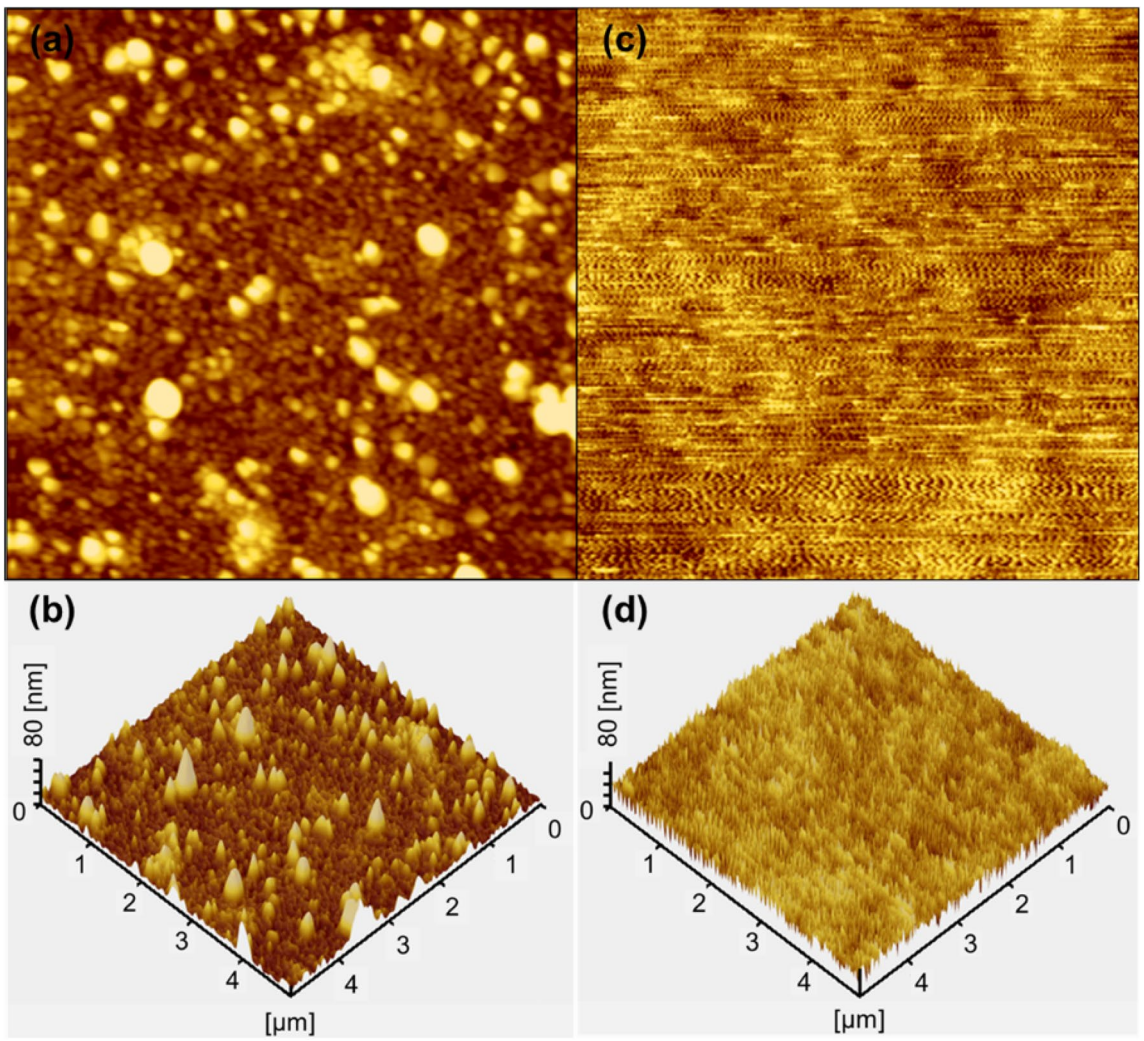

Fig. 6 Analysis of IDE/PDMS under AFM. **a** Optical image of the gap between electrodes reveals the presence of oxide layer with impurities. **b** 3D vision of an oxide layer with sharp-edged particles on the gap surface. **c** Top view of IDE/PDMS. Indicates flat surface with no obvious particle was observed. **d** 3D view. It revealed the smooth surface of IDE/PDMS

the sensitivity with improved flexibility of active elements on the sensing mechanism. In relation to the role of PDMS in the sensing mechanism, the skin hydration level is determined as the IDE/PDMS device was analyzed with different analytes.

Figure 7a shows the results obtained from the reproducibility analysis of IDE/PDMS. The I–V curve shows that the electric signal generated by IDE/PDMS is prominent. The current value was detected at 2 V is 5E-8 A when no sample present on the IDE/PDMS surface. Next, the IDE/PDMS layers were tested with water and the current detected was very low as 5E-9 A, tenfold lesser than the bare IDE/PDMS. Water is poor in conducting electricity and its lower resistance reduces the sensitivity when tested with IDE/PDMS [26]. The bare IDE/PDMS showed high current than water. Since the PDMS layer enables dynamic movements of air particles and biomolecules due to its excellent flexibility and stretching effect, the current generated by the bare IDE/PDMS is observed to be higher than water molecules [27, 28]. Moreover, air particles have high resistance than water, thus IDE/PDMS device-generated high current with air particles than the water molecules. This is further proved by the current curve generated by bare IDE only (Fig. 8). The absence of the PDMS layer disables the rapid and ductile movement of air molecules, thus the bare IDE amplified very low current. When the device was analyzed with pH 4, pH 5, and pH 6, the currents generated were similar to the trend of the current generated when IDE/PDMS was tested

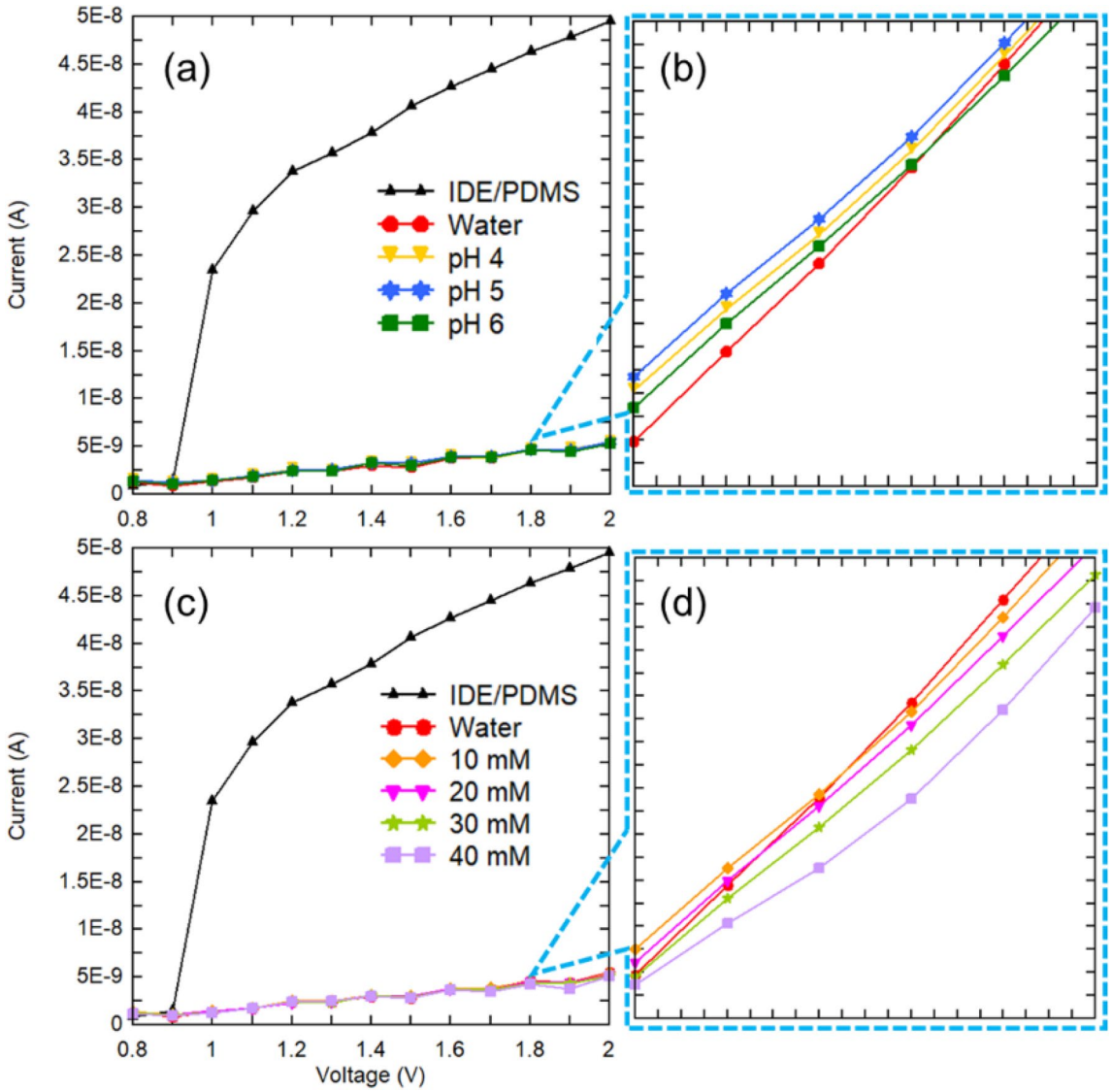

Fig. 7 Electrical characterization of IDE/PDMS. **a** Electrical signal generated by IDE/PDMS at different pH. **b** Enlarged vision of electric current curves of water and electrolytes sample. **c** Electrical signal generated by IDE/PDMS with different urea concentrations. **d** Enlarged vision of electric current curves amplified at different concentrations of urea

with water. The curves emphasize that artificial solution with similar pH as human sweat has no influence on IDE/PDMS sensor. As the current state of art biosensors calls for great in performance devices with very low electrolytes sensitivity, IDE/PDMS is highly recommended for skin hydration detection using sweat samples, moreover for other electrolyte insensitive applications. Figure 7c shows the current generated when urea varies with different concentrations. Sweat secreted from the human body contains about 22 mM urea [29]. The fabricated IDE/PDMS analyzed for the influence of artificial urea concentration by testing the device with 10, 20, 30, and 40 mM urea solutions. Similar to Fig. 6a, there was no prominent current at all concentrations of urea tested with IDE/PDMS and it lies together with the current generated with water. The results obtained when both pH and urea tested with IDE/PDMS affirm that the device has no influence on the presence of artificial sweat and with different pH or urea concentrations. This study implies that IDE/PDMS only gives appropriate results on human sweat and it can be used without the influence of pH and urea concentration in human sweat. Figure 7b and d reveal the enlarged image of I–V curves, showing insensitive current amplification with different concentrations of pH and urea solutions.

3.4 Analysis of human sweat on IDE/PDMS

Figure 8 shows the distinguishing variation of the current generated by IDE/PDMS when it was tested with water, human sweat, and with its bare surface. Human sweat was collected from a male student just after performing physical activity. Sweat is a physiological mixture that contains salt and biomarkers with various types of ions such as Na^+, Ca^{2+}, K^+ and Cl^-. Among them, Na^+ and Cl^- are the most abundant and significant ions which detail the physiological characteristics of secreted sweat [30]. The PDMS layer coated on the Al electrode develops hygroscopic expansion to generate stress on the conductive electrodes. This creates a transition in conductivity, shown as the change of current against supplied voltage since the moisture dependent current increases with increasing humidity [31, 32]. The sensitivity of current also depends on the sweat which directly drop casted sensing surface, based on the amount of ions and charges present in the sample [33]. Sweat has shown prominent current generated by IDE/PDMS, yet it is lower than the current generated by bare IDE/PDMS. The results strongly imply the high-performance IDE/PDMS in contact with human sweat towards the electrical characterization. The high moisture content in sweat reduces the current due to the influence of skin conductivity and dielectric current which will be further analyzed in upcoming studies. The results justify that IDE/PDMS is sensitive only to human sweat and not artificial sweat samples which empowers its performance in skin hydration detections.

Skin hydration level analyzed in terms of impedance or current response against the fixed quantity of supplied voltage using human sweat samples. With the regard, the mechanical strength and durability of the electrode is essential for monitoring non-invasive physiological property

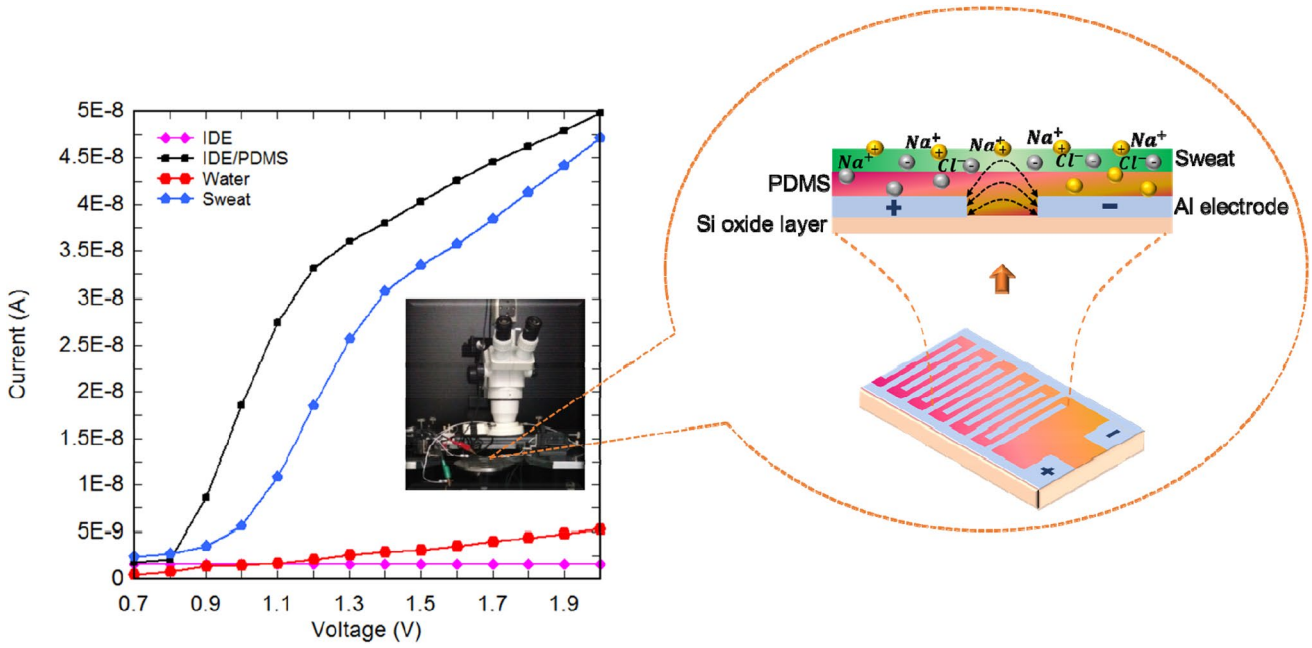

Fig. 8 Evaluation of IDE/PDMS for real-time skin hydration analysis. The current curves represent the variation generated by IDE/PDMS when tested with water and human sweat. Figure inset displays the sensing system

such as skin moisture level. IDE is regarded as a polarizable electrode as it develops large capacitance in contact with any substances [34, 35]. Human skin could not adhere large capacitance from the rigid electrodes. Moreover, IDEs are generally made up of metal electrodes difficult to stand firm against skin contact due to high contact resistance. This would create interruption at the dielectric space between electrode and skin surface, leads to improper conductivity and hydration detection. These reduce the mechanical strength of IDE and the device may lose its tendency for precise skin conductivity analysis [36, 37]. This challenge is easily tackled by developing a flexible polymer on IDE surface to soften the electrode and affirm the fixation between the skin and electrode. As reported in recent technical analyses, PDMS based IDE and other microfluidic devices are mechanically stable in terms of durability and suitability for wearable skin hydration detector. The flexible electrodes enhance the comfort of wearing sensors and provide a better attachment with the skin for monitoring hydration levels [37–40]. In our presented research, we can deduce that the mechanical strength of electrode in terms of its durability and suitability is good as the IDE/PDMS device creates a flexible electrode sensing platform in an approach of real-time non-invasive wearable skin hydration sensor. As illustrated in Fig. 8, the series of current–voltage characterizations performed with IDE/PDMS device justify the appropriate mechanical strength of the sensor in generating a wearable skin hydration sensor.

4 Conclusion

The research has presented a simple, cheap, and flexible skin hydration/dehydration sensor using aluminium IDE with PDMS matrix. The 250 µm aluminium electrode with 400 µm gap sized was successfully fabricated through the conventional photolithography technique. The characterization of fabricated IDE using HPM, SEM, and 3D profiler has affirmed the precision of the low-cost IDE fabrication. PDMS polymer has successfully coated on IDE and the 3D-profiler characterization revealed the thickness of the PDMS matrix to be ~ 40 µm. The polymer-coated surface was further verified by AFM analysis. The electrical characterization of IDE/PDMS implies that the device shows a high-performance in detecting skin hydration as it only gives appropriate results on human sweat. The developed IDE/PDMS has shown zero effect on different concentrations of urea and with different pH. Thus, the presented research justifies the highly efficient PDMS coated IDE in detecting skin hydration/dehydration and encourages the approach of polymer coating on IDE for high-performance electrical characterization without any external influences.

Acknowledgement This work is partly supported by the Ministry of Education Malaysia under the fundamental research grant scheme (FRGS/1/2018/TK04/UNIMAP/02/28), Government of Malaysia.

Compliance with ethical standards

Conflict of interest The authors declare no competing interests.

References

1. R. Wong, S. Geyer, W. Weninger, J.C. Guimberteau, J.K. Wong, Exp. Dermatol. **25**, 92 (2016)
2. Y. Jia, Y. Gan, C. He, Z. Chen, C. Zhou, J. Dermatol. Sci. **89**, 112 (2018)
3. A.J. Bandodkar, P. Gutruf, J. Choi, K.H. Lee, Y. Sekine, J.T. Reeder, W.J. Jeang, A.J. Aranyosi, S.P. Lee, J.B. Model, R. Ghaffari, C.J. Su, J.P. Leshock, T. Ray, A. Verrillo, K. Thomas, V. Krishnamurthi, S. Han, J. Kim, S. Krishnan, T. Hang, J.A. Rogers, Sci. Adv. **5**, 1 (2019)
4. M. Qassem, P. Kyriacou, Cosmetics **6**, 19 (2019)
5. E.H. Mojumdar, Q.D. Pham, D. Topgaard, E. Sparr, Sci. Rep. **7**, 1 (2017)
6. B. Schazmann, D. Morris, C. Slater, S. Beirne, C. Fay, R. Reuveny, N. Moynac, D. Diamondb, Anal. Methods **53**, 1689 (2010)
7. J.T. Reeder, Y. Xue, D. Franklin, Y. Deng, J. Choi, O. Prado, R. Kim, C. Liu, J. Hanson, J. Ciraldo, A.J. Bandodkar, S. Krishnan, A. Johnson, E. Patnaude, R. Avila, Y. Huang, J.A. Rogers, Nat. Commun. **10**, 1 (2019)
8. B. Piro, G. Mattana, V. Noël, Sensors (Switzerland) **19**, 4376 (2019)
9. L.B. Baker, Sport. Med. **47**, 111 (2017)
10. M. Denzinger, S. Krauss, M. Held, L. Joss, J. Kolbenschlag, A. Daigeler, J. Rothenberger, J. Tissue Viability **29**, 2 (2020)
11. M. Dąbrowska, A. Mielcarek, I. Nowak, Ski. Res. Technol. **24**, 614 (2018)
12. S. Jadoon, S. Karim, M. R. Akram, A. Kalsoom Khan, M. A. Zia, A. R. Siddiqi, G. Murtaza, Int. J. Anal. Chem. **2015**, 1687 (2015)
13. T.H. Huang, J.C. Chou, T.P. Sun, S.K. Hsiung, Sens. Actuators B Chem. **134**, 206 (2008)
14. S. Yao, A. Myers, A. Malhotra, F. Lin, A. Bozkurt, J.F. Muth, Y. Zhu, Adv. Healthc. Mater. **6**, 1 (2017)
15. W. Gao, S. Emaminejad, H.Y.Y. Nyein, S. Challa, K. Chen, A. Peck, H.M. Fahad, H. Ota, H. Shiraki, D. Kiriya, D.H. Lien, G.A. Brooks, R.W. Davis, A. Javey, Nature **529**, 509 (2016)
16. S. Ramanathan, S.C.B. Gopinath, M.K.M. Arshad, P. Poopalan, F.K. Loong, T. Lakshmipriya, P. Anbu, Appl. Phys. A **125**, 548 (2019)
17. I. Letchumanan, M.K.M. Arshad, S.C.B. Gopinath, R.D.A.A. Rajapaksha, S.R. Balakrishnan, Sci. Rep. **10**, 1 (2020)
18. H. Adam, S.C.B. Gopinath, M.K.M. Arshad, S. Ramanathan, T. Ashokkumar, M.I.A. Azan, T. Adam, U. Hashim, Appl. Phys. A Mater. Sci. Process. **125**, 1 (2019)
19. S. Ramanathan, S.C.B. Gopinath, M.K.M. Arshad, P. Poopalan, P. Anbu, T. Lakshmipriya, F.H. Kasim, Sci. Rep. **9**, 1 (2019)
20. R.D.A.A. Rajapaksha, U. Hashim, S.C.B. Gopinath, C.A.N. Fernando, Microsyst. Technol. **24**, 1965 (2018)
21. Z. Xu, Y.J. Yuan, Biosens. Bioelectron. **99**, 500 (2018)
22. S. Torino, L. Conte, M. Iodice, G. Coppola, R.D. Prien, Sens. Bio-Sensing Res. **16**, 74 (2017)
23. D. Wang, D. Ba, Z. Hao, Y. Li, F. Sun, K. Liu, G. Du, Q. Mei, Mater. Lett. **221**, 228 (2018)
24. H. Li, J. Zhang, J. Chen, Z. Luo, J. Zhang, Y. Alhandarish, Q. Liu, W. Tang, L. Wang, Sci. Rep. **10**, 1 (2020)

25. S.A. Chowdhury, M.C. Saha, S. Patterson, T. Robison, Y. Liu, Adv. Mater. Technol. **4**, 1 (2019)
26. J. Chouler, M.D. Monti, W.J. Morgan, P.J. Cameron, M. Di Lorenzo, Electrochim. Acta **309**, 392 (2019)
27. Y.L. Tai, Z.G. Yang, J. Mater. Chem. B **3**, 5436 (2015)
28. A. Nag, N. Afasrimanesh, S. Feng, S.C. Mukhopadhyay, Sens. Actuators A Phys. **271**, 257 (2018)
29. R.W. Keller, J.L. Bailey, Y. Wang, J.D. Klein, J.M. Sands, Physiol. Rep. **4**, 1 (2016)
30. J. Yoon, H.-Y. Cho, M. Shin, H. K. Choi, T. Lee, J.-W. Choi, Mater. Chem. B **8**, 7303 (2020)
31. M. Zhang, S. Guo, D. Weller, Y. Hao, X. Wang, C. Ding, K. Chai, B. Zou, R. Liu, J. Nanobiotechnol. **17**, 1 (2019)
32. A. Bhide, S. Muthukumar, A. Saini, S. Prasad, Sci. Rep. **8**, 1 (2018)
33. G. Li, X. Mo, W.C. Law, K.C. Chan, A.C.S. Appl, Mater. Interfaces **11**, 238 (2019)
34. J. Doring, L. Tharmakularajah, K.-L. Krieger, GMA/ITG-Fachtagung Sens. Messsyst. **2019**, 700 (2019)
35. G.A. Hughes, K. Yakal-Kremski, A.V. Call, S.A. Barnett, J. Electrochem. Soc. **159**, F858 (2012)
36. S. Uhm, J. Lee, J. Ind. Eng. Chem. **15**, 661 (2009)
37. Y. Zhao, A. Kim, G. Wan, B. C. K. Tee, Nano Converg. **6**, 2196 (2019)
38. H. Nesser, J. Grisolia, T. Alnasser, B. Viallet, L. Ressier, Nanoscale **10**, 10479 (2018)
39. F. Lu, C. Wang, R. Zhao, L. Du, Z. Fang, X. Guo, Z. Zhao, Biosensors **8**, 31 (2018)
40. M. Fujimaki, K. Nomura, K. Sato, T. Kato, S.C.B. Gopinath, X. Wang, K. Awazu, Y. Ohki, Opt. Express **18**, 15732 (2010)